Multifunctional Thiol-Containing Additives for Improved Photoluminescence and Photovoltaic Performance of $Cs_{0.15}FA_{0.85}PbI_3$ Perovskites

Md Aslam Uddin, Tareq Hossain, Nadeesha L. Kothalawala, Syed Joy, Doo-Young Kim, and Kenneth R. Graham*

Department of Chemistry, University of Kentucky, Lexington, Kentucky 40506, USA

*E-mail: Kenneth.graham@uky.edu

KEYWORDS: *Organic metal halide perovskite, thin films, passivation, photoluminescence, photovoltaics*

ABSTRACT: Thiol containing molecules as both interfacial surface ligands and additives are promising modulators for enhancing photoluminescence (PL) properties, stability, and photovoltaic (PV) performance of metal halide perovskites. However, alkanethiols are much more effective for improving photoluminescence (PL) intensity and stability in metal halide perovskite nanocrystals than in their thin film analogues. Herein, we investigate how additional functional groups on a pyrimidine core can alter thiol reactivity and influence the PL, stability, and PV performance of organic metal halide perovskites. Through an investigation of five different pyrimidine derivatives, it is shown that all derivatives containing thiol groups form thiolates in the presence of the perovskite precursors and increase the photoluminescence intensity of the perovskite film. The largest all-around improvement to the PL intensity, stability, and photovoltaic performance of $Cs_{0.15}FA_{0.85}PbI_3$ perovskites is realized through the addition of a hydroxyl group combined with a trifluoromethyl group to form 4-hydroxy-6-(trifluoromethyl)pyrimidine-2-thiol. This investigation helps illuminate how combinations of functional groups can be employed to further increase the beneficial effects over mono-functional additives in organic metal halide perovskites.

Organic metal halide perovskites (HPs) are pioneering light harvesting materials for photovoltaics (PVs) and light-emitting applications.[1,2] However, these materials suffer from poor stability and there is further room for improving their performance in both PVs and light emitting applications.[3,4] In addition, they are prone to degradation under electron beam irradiation,[5] humidity,[6] heat,[7] and light.[8] Introducing interfacial surface ligands and solution additives are promising routes to enhance stability and PL properties of both HP nanocrystals (NCs) and thin films, as these ligands and additives can passivate defect states. Passivation can be performed on both NCs and thin films in different ways: including introducing additives in the precursor solution used for synthesis of NCs or thin films and exposing the NCs or thin films to surface ligands in solution or in the vapor phase post-synthesis.[9–13] Passivation of both NCs and their bulk counterparts have been investigated with different ligand binding groups, including thiols,[10,13–19] trichlorosilanes,[20–22] alkoxysilanes,[23–26] phosphonic acids,[27–29] carboxylic acids,[28,30,31] zwitterionic ligands,[32,33] ammonium ligands,[34–37] and other salts (e.g., NaSCN, NH_4SCN, $NaBF_4$, NH_4BF_4, etc.).[11,38] Among these passivating groups, thiols are promising passivants for metal-halide perovskite NCs and their bulk counterparts because of the coordinating nature of thiolate ions toward undercoordinated Pb atoms,[39] which results in enhanced optical and electronic properties of metal-halide perovskites upon thiol treatment.[10,16,40]

Thiols as interfacial ligands are effective in reducing recombination at interfaces between perovskites and charge transport layers. It was demonstrated that incorporation of 4-mercaptobenzoic acid at the $TiO_2/MAPbI_3$ interface facilitates electron transfer from $MAPbI_3$ to TiO_2 and alters the HP film morphology to enhance the power conversion efficiency (PCE) of PV devices,[13] whereas treatment of $MAPbI_3$ thin films at the $MAPbI_3$/Spiro-OMeTAD interface with pentafluorobenzenethiol improves the overall stability of the PV devices.[13] In other surface modification studies, thiol-functionalized molecules were used to modify HP films and found to improve the device performance via suppressing undercoordinated Pb and Pb^0 formation, as well as to improve stability via suppressing phase segregation in the HP.[41,42] In the alternative approach, where thiols are added directly to the HP precursor solutions, thiol-based additives such as mercapto-tetrazolium in $Cs_xFA_{1-x}PbI_3$ and 1-dodecanethiol in $(FAPbI_3)_{0.85}(MAPbBr_3)_{0.15}$, respectively, were demonstrated to passivate surface defects and promote the formation of larger grains; thereby, enhancing PV performance and operational stability under ambient conditions.[10,43]

In our previous study, we also explored the role of thiols in enhancing the PL quantum yield (Φ_{PL}) and stability of HP NCs.[15,16] We show that alkanethiols are able to enhance the Φ_{PL} of as-synthesized $CsPbCl_3$ (Φ_{PL} of <1%) and $CsPbBr_3$ NCs (Φ_{PL} of <50%) to near 50% and 100% for $CsPbCl_3$ and $CsPbBr_3$, respectively, and greatly improve the stability.[15,16] However, we find that these

benefits are drastically reduced when alkanethiols are used with HP thin films. Herein, we investigate a family of pyrimidine derivatives, including thiol substituted derivatives, to determine how varying substituents influence the effectiveness of thiols in passivating defect states, improving film stability, and increasing the PV performance of $Cs_{0.15}FA_{0.85}PbI_3$ based cells. We find that 4-hydroxy-6-(trifluoromethyl)pyrimidine-2-thiol (P-CF_3-OH-SH) results in the largest increase in the PL intensity and PV performance, while also improving the stability of $Cs_{0.15}FA_{0.85}PbI_3$ thin films. These improvements are attributed to suppression of undercoordinated lead atoms in thin film surfaces and grain boundaries left by the excess PbI_2 containing precursor solution, as supported by x-ray diffraction (XRD). The greater improvement of P-CF_3-OH-SH relative to the other pyrimidines is attributed to the combination of the electron withdrawing trifluoromethyl substituent and the hydroxyl group.

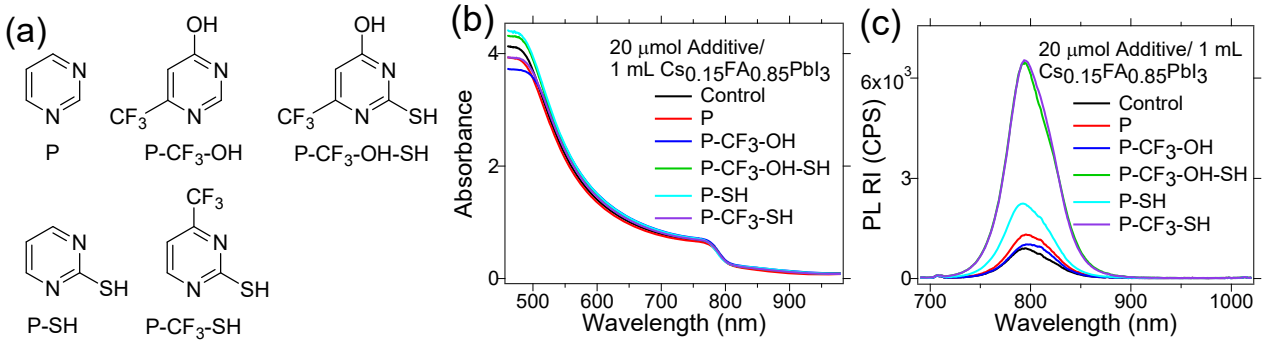

Figure 1. (a) Structures of the additives investigated and **(b)** absorbance and **(c)** PL relative intensity (RI) spectra of fabricated $Cs_{0.15}FA_{0.85}PbI_3$ thin films on glass substrates with 20 µmol of each ligand added in the precursor solutions.

In this work, $Cs_{0.15}FA_{0.85}PbI_3$ thin films were fabricated with 5% PbI_2 excess with respect to 1.3 M concentration of perovskite precursor solution. This composition was selected due to its superior stability relative to pure $MAPbI_3$ or $FAPbI_3$, while excess PbI_2 was included as it is reported to benefit $Cs_{0.05}(FA_{0.83}MA_{0.17})_{0.95}Pb(I_{0.83}Br_{0.17})_3$,[44] $MAPbI_3$,[45,46] and $Cs_xFA_{1-x}PbI_3$ PVs.[47] We find an excess of 5% PbI_2 delivers the highest PL intensity and PV performance, as shown in **Figure S1**. The series of multifunctional additives investigated are depicted in **Figure 1a** and include pyrimidine (P), 4-hydroxy-6-(trifluoromethyl)-pyrimidine (P-CF_3-OH), 4-hydroxy-6-(trifluoromethyl)pyrimidine-2-thiol (P-CF_3-OH-SH), 2-mercaptopyrimidine (P-SH), and 2-mercapto-4-(trifluoromethyl)pyrimidine (P-CF_3-SH). Complete details of thin film and PV device fabrication are found in the experimental section.

An optimal additive concentration was determined to be 20 µmol additive to 1 mL of $Cs_{0.15}FA_{0.85}PbI_3$ precursor solution based on both PL intensity and PV device performance, as shown in **Figure S2 and S3**, respectively. Thus, all data discussed herein is based on the additives at a 20 mM concentration in the $Cs_{0.15}FA_{0.85}PbI_3$ precursor solution, which equates to an additive to PbI_2 molar ratio of *ca*. 0.015. Absorbance and PL spectra of the HP thin films with each additive are shown in **Figure 1b & c.** No significant change is observed in the absorbance spectra with the varying additives, indicating that the $Cs_{0.15}FA_{0.85}PbI_3$ structure remains intact. On the other hand, the PL intensity of the thin films with the different additives varies significantly. All additives show an enhancement in PL intensity compared to the control film. For P and P-CF_3-OH, where no thiol is present, the increase in PL intensity is the smallest. The addition of the thiol group in P-SH results in a larger increase in PL intensity, but this increase in intensity is still dwarfed relative to when both the thiol and electron withdrawing trifluoromethyl group are present (P-CF_3-OH-SH and P-CF_3-SH). For both P-CF_3-SH and P-CF_3-OH-SH, the PL intensity increases 7-fold with 2-8 nm red shifts in PL maxima, as shown in **Figure 1c & S4**.

Photovoltaic devices with a *p-i-n* architecture (glass/ITO/$Cs_{0.15}FA_{0.85}PbI_3$/C_{60}/BCP/Al) were fabricated with the varying pyrimidine derivatives. The J-V characteristics and PV device parameters are presented in **Figure 2b and S5a-d**, respectively. From **Figure S5a-d**, it is seen that pyrimidine (P), P-CF_3-OH, and P-CF_3-SH show similar device performance, whereas P-SH shows the poorest device performance. The relatively low PV performance with P-SH is attributed to a worse film morphology consisting of frequent pinholes, as indicated in the scanning electron microscope (SEM) images shown in **Figure S6f**. Although both P-CF_3-OH-SH and P-CF_3-SH show a 7-fold enhancement in PL intensity, PV devices with P-CF_3-SH display lower performance compared with P-CF_3-OH-SH, which is attributed to the presence of pinholes.[48] P-CF_3-OH-SH as an additive reproducibly shows a higher average PCE of 16.4±0.7% compared to that of control devices (average PCE of 15.1±0.7%), as shown in **Figure 2 and S5,** and a champion PCE of 18.2%. This PCE improvement with P-CF_3-OH-SH comes from an enhancement in both J_{sc} and V_{oc}. Both the higher J_{sc} and

V_{oc} indicate suppressed charge recombination in the HP layer and/or at the HP/transport layer interfaces,[49] which is consistent with the increased PL intensity relative to the control $Cs_{0.15}FA_{0.85}PbI_3$ film.

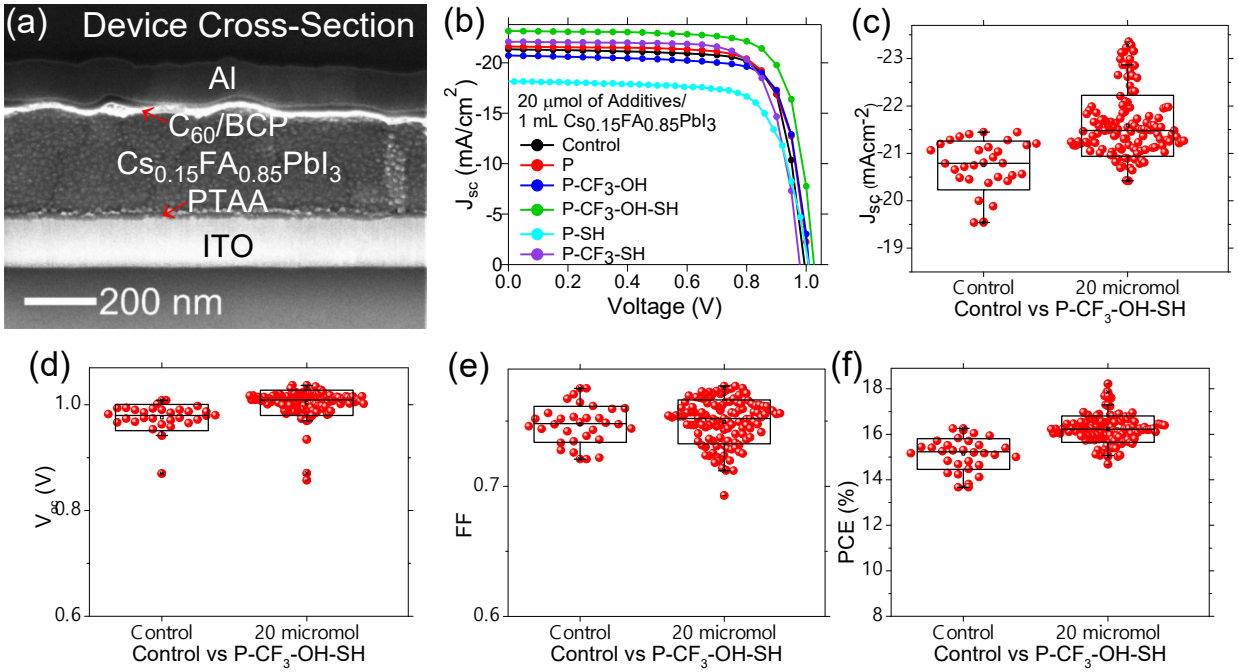

Figure 2. (**a**) SEM cross-section of *p-i-n* PV device (glass-ITO/PTAA/$Cs_{0.15}FA_{0.85}PbI_3$/C_{60}/BCP/Al), **(b)** J-V characteristics of $Cs_{0.15}FA_{0.85}PbI_3$ thin film PVs, fabricated with and without different additives in the perovskite precursor solution, under AM 1.5 G illumination; and **(c-f)** PV performance parameters under 1 sun illumination of the control device and with 20 mM P-CF_3-OH-SH. In **Figure 2c-f**, each red dot indicates an individual PV cell with active area of 0.1 cm^2.

The XRD and transmission electron microscopy (TEM) images show no detectable changes in the $Cs_{0.15}FA_{0.85}PbI_3$ crystal structure with varying additives. Here, peak positions from $Cs_{0.15}FA_{0.85}PbI_3$ remain consistent and d-spacing values from high-resolution TEM crystal fringes of the control (d_{200} = 0.315±0.012 nm) and P-CF_3-OH-SH added films (d_{200} = 0.313±0.015 nm) remain nearly identical, as shown in **Figure S7**.[50] The main observation from the XRD spectra is that the intensity of the PbI_2 peak at 12.6° is reduced upon incorporation of all additives, as shown in **Figure S7 and S8a, b**. This reduction in PbI_2 may arise from the stabilizing effects of the additives, as PbI_2 is a known decomposition product,[47] or the reduction of the initial amount of PbI_2 formed as a result of PbI_2 coordination in solution and during film formation. We also find that P-CF_3-OH-SH increases the $Cs_{0.15}FA_{0.85}PbI_3$ stability under TEM electron beam irradiation compared to that of the control film, as demonstrated in **Figure S9**. This improved stability is also evident in the PV devices, which showed improved stability upon storage at ambient and elevated (65 °C) temperatures, as shown in **Figure S10**.

The additive may accumulate at grain boundaries, including the top and bottom interfaces, be incorporated into the crystalline grains, or largely excluded from the formed $Cs_{0.15}FA_{0.85}PbI_3$ films. To determine the distribution of P-CF_3-OH-SH in the $Cs_{0.15}FA_{0.85}PbI_3$ films, we collected STEM elemental mapping images of $Cs_{0.15}FA_{0.85}PbI_3$ film sections, as shown in **Figure S11**. Based on the distribution of fluorine and sulfur elements, we observe that P-CF_3-OH-SH does not accumulate at grain boundaries and is either distributed throughout the HP grains or as a uniform coating over the exposed surfaces.

The original hypothesis of the work was that the pyrimidine and substituent groups could play an auxilary role of activating the thiol and also coordinating with the $Cs_{0.15}FA_{0.85}PbI_3$ precursors. To obtain more information regarding the presence and role of P-CF_3-OH-SH in perovskite solid films, we collected XPS and NMR data. XPS measurements shown in **Figure S12** indicate that there is not a detectable layer of P-CF_3-OH-SH on the film surface, and NMR studies strongly support that the thiol group in P-CF_3-OH-SH is deprotonated in solution.

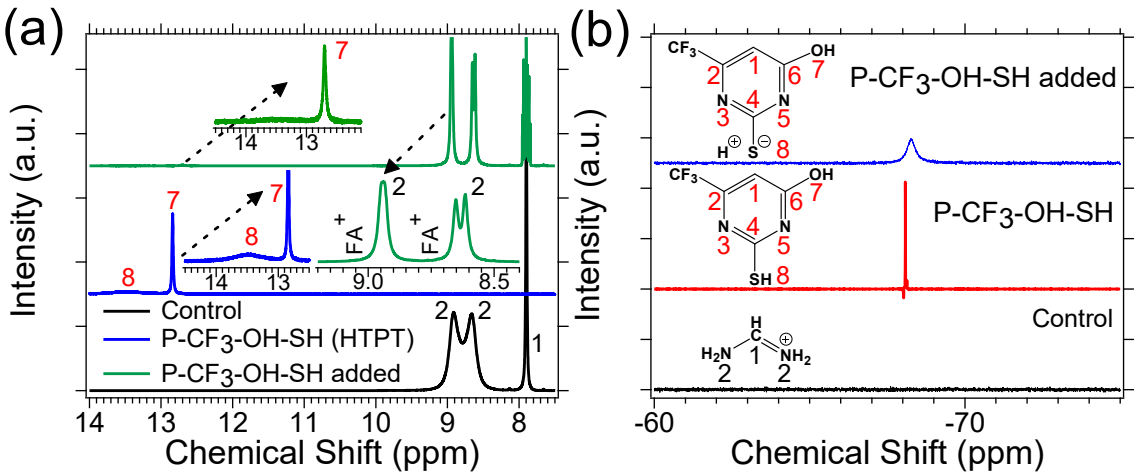

Figure 3. **(a)** ^{1}H NMR and **(b)** ^{19}F NMR of the $Cs_{0.15}FA_{0.85}PbI_3$ precursor solution (control), P-CF_3-OH-SH solution, and $Cs_{0.15}FA_{0.85}PbI_3$ precursor solution with P-CF_3-OH-SH added. All spectra were recorded in deuterated DMSO.

The ^{1}H NMR of FA^+ shows two broad proton peaks 2 at 8.66 and 8.91 ppm, respectively, as indicated in **Figure 3a and S13**. These same peaks are absent from the ^{1}H NMR of the pure P-CF_3-OH-SH molecule. When P-CF_3-OH-SH is added to the HP precursor solution the FA^+ peaks change significantly. Here, the 8.63 peak splits into a doublet, the second NH_2 peak at 8.9 ppm narrows considerably, and the CH peak at 7.9 ppm splits into a triplet of triplets when P-CF_3-OH-SH is added. The increased peak resolution is attributed to increased solution acidity and decreased proton exchange between the NH_2/NH_2^+ groups and water in solution.[51] This conclusion is further supported by the peak shift of protons from H_2O/H_3O^+ from 3.35 and 3.45 for the P-CF_3-OH-SH and $Cs_{0.15}FA_{0.85}PbI_3$ precursor solutions, respectively, to 3.62 ppm for the $Cs_{0.15}FA_{0.85}PbI_3$ precursor with P-CF_3-OH-SH added. The absence of the thiol proton (peak 8) after P-CF_3-OH-SH is added to the $Cs_{0.15}FA_{0.85}PbI_3$ precursor solution confirms that P-CF_3-OH-S^- forms.

The ^{1}H NMR spectra of P-SH, P-CF_3-SH, and P-CF_3-OH individually and in the $Cs_{0.15}FA_{0.85}PbI_3$ precursor solution were also recorded, as shown in **Figure S15** and **S16**. Here, we see that both P-SH and P-CF_3-SH are also deprotonated to form the thiolate in the precursor solution and the solution becomes more acidic, as indicated by the lack of NMR signal from the thiol protons for both thiols and a shift in the water peak to 4.02 ppm, respectively, in the precursor solution with P-CF_3-SH. When the thiol is removed and only the hydroxyl and CF_3 groups are present in P-CF_3-OH, the precursor solution does not become acidic, and the hydroxyl group is not deprotonated. Another observation from the NMR is that the protons off the 6 C or 2 and 6 C (as labeled in Figure 3a for P-CF_3-OH-SH) in P-CF_3-SH and P-SH, respectively, at near 8.3 ppm are not apparent when these additives are present in the precursor solution (Figure S15 and S16). It is possible that these protons shift when the thiolate forms to be hidden by the FA peaks, or that these proton signals broaden significantly due to interactions with PbI_2 or PbI_2 and H_2O. The incorporation of H_2O in the complex is supported by broadening of the H_2O/H_3O^+ peak in the $Cs_{0.15}FA_{0.85}PbI_3$ precursor solution with P-CF_3-SH and the disappearance of the H_2O/H_3O^+ peak altogether with P-SH. In summary, the NMR spectra show that all thiol containing pyrimidines are deprotonated in solution, but the influence of the pyrimidine derivatives extends beyond thiol deprotonation to include additional solution phase intermolecular and H-bonding interactions.

The solution phase interactions and formation of complexes is also supported by ^{19}F NMR spectra of P-CF_3-OH-SH in the absence and presence of the $Cs_{0.15}FA_{0.15}PbI_3$ precursor, as shown in **Figure 3b and S14**. Here, these spectra show that the F peak broadens when P-CF_3-OH-SH is added to the $Cs_{0.15}FA_{0.85}PbI_3$ precursor solution. We attribute this broadening to the interaction of P-CF_3-OH-S^- with PbI_2 in the perovskite precursor solution.

To better understand the impact of P-CF_3-OH-SH and P-CF_3-SH on the electronic properties of the HP films, we collected UPS spectra of the HP films with these two additives. **Figure 4** shows the UPS spectra of a control HP film, HP film with P-CF_3-OH-SH added, and HP film with P-CF_3-SH added. It is found that the work function decreases by approximately 0.15 eV when either of these additives is included and the ionization energies (IEs) decrease from 6.07 to 5.94 eV, which could arguably improve charge carrier extraction. All films are more *n*-type, as indicated by the large difference between the work function and IE. From an energetic perspective, there is no reason that P-CF_3-SH should show lower PV performance than P-CF_3-OH-SH, which combined with the PL results supports the previous discussion that the lower PV performance with P-CF_3-SH relative to P-CF_3-OH-SH is attributed to morphological differences.

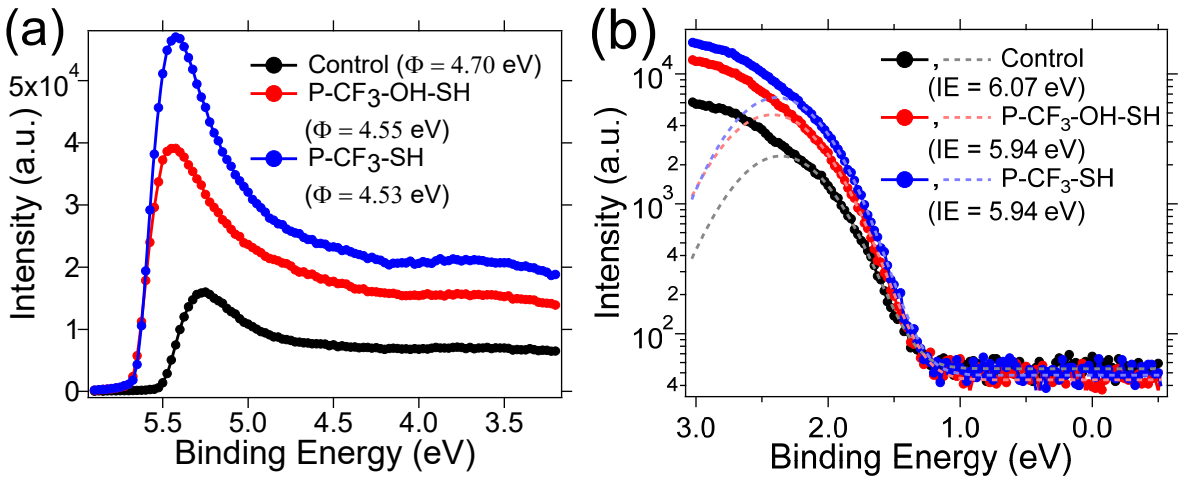

Figure 4. UPS spectra showing the **(a)** secondary electron cut-off region (10.2 eV photon source) and the **(b)** valence band onset region with Gaussian fittings of the control HP film, HP film with P-CF_3-OH-SH added, and HP film with P-CF_3-SH added. The work functions (Φ) and IEs are indicated on the spectra.

In summary, the role of multifunctional pyrimidine additives on the PL properties and PV performance of $Cs_{0.15}FA_{0.85}PbI_3$ is explored. We find that the substituents off of the pyrimidine ring have a large effect on both the PL and PV properties, with 4-hydroxy-6-(trifluoromethyl)pyridimidine-2-thiol (P-CF_3-OH-SH) greatly enhancing the PL intensity and PV performance of $Cs_{0.15}FA_{0.85}PbI_3$ perovskite thin films. The increased PL properties and PV performance are attributed to formation of thiolate in the HP precursor solution and likely coordination between the thiolate and PbI_2 in solution, which reduces the defect states present in the HP films. The presence of a CF_3 group is shown to be critical to increasing the additives effectiveness, as without this CF_3 group the PL intensity is only approximately one-third as intense as it is when both a CF_3 and thiol group are included. In general, this work highlights the interplay of functional groups in tuning the reactivity of additives in HPs.

ASSOCIATED CONTENT

UV-Vis absorbance & PL spectra, SEM and TEM images, X-ray diffraction spectra, J-V curves and device statistics, and NMR spectra are included in the Supporting Information.

AUTHOR INFORMATION

Corresponding Author

* E-mail: kenneth.graham@uky.edu

Author Contributions

The manuscript was written through contributions of all authors. All authors have given approval to the final version of the manuscript.

Notes

The authors declare no competing financial interest.

ACKNOWLEDGMENT

This work, including funding for M.A.U., T.H., and K.R.G., was primarily supported by the U.S. Department of Energy, Office of Science, Basic Energy Sciences under Award Number DE-SC0018208. M.A.U., T.H., S.J., and K.R.G. acknowledge support for the NMR, SEM, and partial PV device optimization from the National Science Foundation under cooperative agreement No. 1849213. D.Y.K and N.L.K appreciate the support from Samsung Global Research Outreach (GRO) program. N.L.K appreciate the support from a Research Challenge Trust Fund.

ABBREVIATIONS

PL, photoluminescence; PV, photovoltaics; PCE, power conversion efficiency; HP, halide perovskites.

REFERENCES

(1) Kojima, A.; Teshima, K.; Shirai, Y.; Miyasaka, T. Organometal Halide Perovskites as Visible-Light Sensitizers for Photovoltaic Cells. *J. Am. Chem. Soc.* **2009**, *131* (17), 6050–6051.

(2) Tan, Z.-K.; Moghaddam, R. S.; Lai, M. L.; Docampo, P.; Higler, R.; Deschler, F.; Price, M.; Sadhanala, A.; Pazos, L. M.; Credgington, D.; Hanusch, F.; Bein, T.; Snaith, H. J.; Friend, R. H. Bright Light-Emitting Diodes Based on Organometal Halide Perovskite. *Nat. Nanotechnol.* **2014**, *9* (9), 687–692.

(3) Wang, D.; Wright, M.; Elumalai, N. K.; Uddin, A. Stability of Perovskite Solar Cells. *Sol. Energy Mater. Sol. Cells* **2016**, *147*, 255–275.

(4) Meng, L.; You, J.; Yang, Y. Addressing the Stability Issue of Perovskite Solar Cells for Commercial Applications. *Nat. Commun.* **2018**, *9* (1), 1–4.

(5) Dang, Z.; Shamsi, J.; Palazon, F.; Imran, M.; Akkerman, Q. A.; Park, S.; Bertoni, G.; Prato, M.; Brescia, R.; Manna, L. In Situ Transmission Electron Microscopy Study of Electron Beam-Induced Transformations in Colloidal Cesium Lead Halide Perovskite Nanocrystals. *ACS Nano* **2017**, *11* (2), 2124–2132.

(6) Yang, J.; Siempelkamp, B. D.; Liu, D.; Kelly, T. L. Investigation of CH3NH3PbI3 Degradation Rates and Mechanisms in

Controlled Humidity Environments Using in Situ Techniques. *ACS Nano* **2015**, *9* (2), 1955–1963.

(7) Conings, B.; Drijkoningen, J.; Gauquelin, N.; Babayigit, A.; D'Haen, J.; D'Olieslaeger, L.; Ethirajan, A.; Verbeeck, J.; Manca, J.; Mosconi, E.; De Angelis, F.; Boyen, H. G. Intrinsic Thermal Instability of Methylammonium Lead Trihalide Perovskite. *Adv. Energy Mater.* **2015**, *5* (15), 1–8.

(8) Farooq, A.; Hossain, I. M.; Moghadamzadeh, S.; Schwenzer, J. A.; Abzieher, T.; Richards, B. S.; Klampaftis, E.; Paetzold, U. W. Spectral Dependence of Degradation under Ultraviolet Light in Perovskite Solar Cells. *ACS Appl. Mater. Interfaces* **2018**, *10* (26), 21985–21990.

(9) Protesescu, L.; Yakunin, S.; Bodnarchuk, M. I.; Krieg, F.; Caputo, R.; Hendon, C. H.; Yang, R. X.; Walsh, A.; Kovalenko, M. V. Nanocrystals of Cesium Lead Halide Perovskites (CsPbX3, X = Cl, Br, and I): Novel Optoelectronic Materials Showing Bright Emission with Wide Color Gamut. *Nano Lett.* **2015**, *15* (6), 3692–3696.

(10) Bi, D.; Li, X.; Milić, J. V.; Kubicki, D. J.; Pellet, N.; Luo, J.; LaGrange, T.; Mettraux, P.; Emsley, L.; Zakeeruddin, S. M.; Grätzel, M. Multifunctional Molecular Modulators for Perovskite Solar Cells with over 20% Efficiency and High Operational Stability. *Nat. Commun.* **2018**, *9* (1), 1–10.

(11) Koscher, B. A.; Swabeck, J. K.; Bronstein, N. D.; Alivisatos, A. P. Essentially Trap-Free CsPbBr3 Colloidal Nanocrystals by Postsynthetic Thiocyanate Surface Treatment. *J. Am. Chem. Soc.* **2017**, *139* (19), 6566–6569.

(12) Boehm, A. M.; Liu, T.; Park, S. M.; Abtahi, A.; Graham, K. R. Influence of Surface Ligands on Energetics at FASnI3/C60 Interfaces and Their Impact on Photovoltaic Performance. *ACS Appl. Mater. Interfaces* **2019**, *12* (5), 5209–5218.

(13) Cao, J.; Yin, J.; Yuan, S.; Zhao, Y.; Li, J.; Zheng, N. Thiols as Interfacial Modifiers to Enhance the Performance and Stability of Perovskite Solar Cells. *Nanoscale* **2015**, *7* (21), 9443–9447.

(14) Ruan, L.; Shen, W.; Wang, A.; Xiang, A.; Deng, Z. Alkyl-Thiol Ligand-Induced Shape- and Crystalline Phase-Controlled Synthesis of Stable Perovskite-Related CsPb2Br5Nanocrystals at Room Temperature. *J. Phys. Chem. Lett.* **2017**, *8* (16), 3853–3860.

(15) Uddin, M. A.; Glover, J. D.; Park, S. M.; Pham, J. T.; Graham, K. R. Growth of Highly Stable and Luminescent CsPbX3 (X = Cl, Br, and I) Nanoplates via Ligand Mediated Anion Exchange of CsPbCl3 Nanocubes with AlX3. *Chem. Mater.* **2020**, *32* (12), 5217–5225.

(16) Uddin, M. A.; Mobley, J. K.; Masud, A. Al; Liu, T.; Calabro, R. L.; Kim, D.-Y.; Richards, C. I.; Graham, K. R. Mechanistic Exploration of Dodecanethiol Treated Colloidal CsPbBr3 Nanocrystals With Photoluminescence Quantum Yields Reaching Near 100%. *J. Phys. Chem. C* **2019**, *123* (29), 18103–18112.

(17) Ruan, L.; Shen, W.; Wang, A.; Zhou, Q.; Zhang, H.; Deng, Z. Stable and Conductive Lead Halide Perovskites Facilitated by X-Type Ligands. *Nanoscale* **2017**, *9* (21), 7252–7259.

(18) Liu, Z.; Bekenstein, Y.; Ye, X.; Nguyen, S. C.; Swabeck, J.; Zhang, D.; Lee, S.-T.; Yang, P.; Ma, W.; Alivisatos, A. P. Ligand Mediated Transformation of Cesium Lead Bromide Perovskite Nanocrystals to Lead Depleted Cs4PbBr6 Nanocrystals. *J. Am. Chem. Soc.* **2017**, *139* (15), 5309–5312.

(19) Chang, C. Y.; Chang, Y. C.; Huang, W. K.; Liao, W. C.; Wang, H.; Yeh, C.; Tsai, B. C.; Huang, Y. C.; Tsao, C. S. Achieving High Efficiency and Improved Stability in Large-Area ITO-Free Perovskite Solar Cells with Thiol-Functionalized Self-Assembled Monolayers. *J. Mater. Chem. A* **2016**, *4* (20), 7903–7913.

(20) Uddin, M. A.; Calabro, R. L.; Kim, D. Y.; Graham, K. R. Halide Exchange and Surface Modification of Metal Halide Perovskite Nanocrystals with Alkyltrichlorosilanes. *Nanoscale* **2018**, *10* (35), 16919–16927.

(21) Torun, I.; Altintas, Y.; Yazici, A. F.; Mutlugun, E.; Onses, M. S. Solid-State Encapsulation and Color Tuning in Films of Cesium Lead Halide Perovskite Nanocrystals for White Light Generation. *ACS Appl. Nano Mater.* **2019**, *2* (3), 1185–1193.

(22) Wang, J.; Xiang, X.; Yao, X.; Xiao, W. J.; Lin, J.; Li, W. S. Efficient Perovskite Solar Cells Using Trichlorosilanes as Perovskite/PCBM Interface Modifiers. *Org. Electron.* **2016**, *39*, 1–9.

(23) Liu, Z.; Zhang, Y.; Fan, Y.; Chen, Z.; Tang, Z.; Zhao, J.; Lv, Y.; Lin, J.; Guo, X.; Zhang, J.; Liu, X. Toward Highly Luminescent and Stabilized Silica-Coated Perovskite Quantum Dots through Simply Mixing and Stirring under Room Temperature in Air. *ACS Appl. Mater. Interfaces* **2018**, *10* (15), 13053–13061.

(24) Li, S.; Lei, D.; Ren, W.; Guo, X.; Wu, S.; Zhu, Y.; Rogach, A. L.; Chhowalla, M.; Jen, A. K. Y. Water-Resistant Perovskite Nanodots Enable Robust Two-Photon Lasing in Aqueous Environment. *Nat. Commun.* **2020**, *11* (1), 1–8.

(25) Sun, C.; Zhang, Y.; Ruan, C.; Yin, C.; Wang, X.; Wang, Y.; Yu, W. W. Efficient and Stable White LEDs with Silica-Coated Inorganic Perovskite Quantum Dots. *Adv. Mater.* **2016**, *28* (45), 10088–10094.

(26) Luo, B.; Pu, Y. C.; Lindley, S. A.; Yang, Y.; Lu, L.; Li, Y.; Li, X.; Zhang, J. Z. Organolead Halide Perovskite Nanocrystals: Branched Capping Ligands Control Crystal Size and Stability. *Angew. Chemie - Int. Ed.* **2016**, *55* (31), 8864–8868.

(27) Lu, J.; Lin, X.; Jiao, X.; Gengenbach, T.; Scully, A. D.; Jiang, L.; Tan, B.; Sun, J.; Li, B.; Pai, N.; Bach, U.; Simonov, A. N.; Cheng, Y. B. Interfacial Benzenethiol Modification Facilitates Charge Transfer and Improves Stability of Cm-Sized Metal Halide Perovskite Solar Cells with up to 20% Efficiency. *Energy Environ. Sci.* **2018**, *11* (7), 1880–1889.

(28) Nenon, D. P.; Pressler, K.; Kang, J.; Koscher, B. A.; Olshansky, J. H.; Osowiecki, W. T.; Koc, M. A.; Wang, L.-W.; Alivisatos, A. P. Design Principles for Trap-Free CsPbX3 Nanocrystals: Enumerating and Eliminating Surface Halide Vacancies with Softer Lewis Bases. *J. Am. Chem. Soc.* **2018**, *140* (50), 17760–17772.

(29) Zhang, B.; Goldoni, L.; Zito, J.; Dang, Z.; Almeida, G.; Zaccaria, F.; Wit, J. De; Infante, I.; Trizio, L. De; Manna, L. Alkyl Phosphonic Acids Deliver CsPbBr3 Nanocrystals with High Photoluminescence Quantum Yield and Truncated Octahedron Shape. *Chem. Mater.* **2019**, *31* (21), 9140–9147.

(30) Pan, J.; Shang, Y.; Yin, J.; De Bastiani, M.; Peng, W.; Dursun, I.; Sinatra, L.; El-Zohry, A. M.; Hedhili, M. N.; Emwas, A. H.; Mohammed, O. F.; Ning, Z.; Bakr, O. M. Bidentate Ligand-Passivated CsPbI3 Perovskite Nanocrystals for Stable Near-Unity Photoluminescence Quantum Yield and Efficient Red Light-Emitting Diodes. *J. Am. Chem. Soc.* **2018**, *140* (2), 562–565.

(31) Alpert, M. R.; Niezgoda, J. S.; Chen, A. Z.; Foley, B. J.; Cuthriell, S.; Yoon, L. U.; Choi, J. J. Colloidal Nanocrystals as a Platform for Rapid Screening of Charge Trap Passivating Molecules for Metal Halide Perovskite Thin Films. *Chem. Mater.* **2018**, *30* (14), 4515–4526.

(32) Krieg, F.; Ochsenbein, S. T.; Yakunin, S.; Ten Brinck, S.; Aellen, P.; Süess, A.; Clerc, B.; Guggisberg, D.; Nazarenko, O.; Shynkarenko, Y.; Kumar, S.; Shih, C. J.; Infante, I.; Kovalenko, M. V. Colloidal CsPbX3 (X = Cl, Br, I) Nanocrystals 2.0: Zwitterionic Capping Ligands for Improved Durability and Stability. *ACS Energy Lett.* **2018**, *3* (3), 641–646.

(33) Jancik Prochazkova, A.; Demchyshyn, S.; Yumusak, C.; Másilko, J.; Brüggemann, O.; Weiter, M.; Kaltenbrunner, M.; Sariciftci, N. S.; Krajcovic, J.; Salinas, Y.; Kovalenko, A. Proteinogenic Amino Acid Assisted Preparation of Highly Luminescent Hybrid Perovskite Nanoparticles. *ACS Appl. Nano Mater.* **2019**, *2* (7), 4267–4274.

(34) Zhang, H.; Wu, Y.; Shen, C.; Li, E.; Yan, C.; Zhang, W.; Tian, H.; Han, L.; Zhu, W. Efficient and Stable Chemical Passivation on Perovskite Surface via Bidentate Anchoring. *Adv. Energy Mater.* **2019**, *9* (13), 1803573.

(35) Hoshi, K.; Chiba, T.; Sato, J.; Hayashi, Y.; Takahashi, Y.; Ebe, H.; Ohisa, S.; Kido, J. Purification of Perovskite Quantum Dots Using Low-Dielectric-Constant Washing Solvent "Diglyme" for Highly Efficient Light-Emitting Devices. *ACS Appl. Mater. Interfaces* **2018**, *10* (29), 24607–24612.

(36) Chiba, T.; Hoshi, K.; Pu, Y. J.; Takeda, Y.; Hayashi, Y.; Ohisa, S.; Kawata, S.; Kido, J. High-Efficiency Perovskite Quantum-Dot Light-Emitting Devices by Effective Washing Process and Interfacial Energy Level Alignment. *ACS Appl. Mater. Interfaces* **2017**, *9* (21), 18054–18060.

(37) Moyen, E.; Jun, H.; Kim, H.; Jang, J. Surface Engineering of Room Temperature-Grown Inorganic Perovskite Quantum Dots for Highly Efficient Inverted Light- Emitting Diodes. *ACS Appl. Mater. Interfaces* **2018**, *10* (49), 42647–42656.

(38) Ahmed, T.; Seth, S.; Samanta, A. Boosting the Photoluminescence of CsPbX3(X = Cl, Br, I) Perovskite Nanocrystals Covering a Wide Wavelength Range by Postsynthetic Treatment with Tetrafluoroborate Salts. *Chem. Mater.* **2018**, *30* (11), 3633–3637.

(39) Tolbatov, I.; Marrone, A. Molecular Dynamics Simulation of the Pb(II) Coordination in Biological Media via Cationic Dummy Atom Models. *Theor. Chem. Acc.* **2021**, *140* (2), 1–12.

(40) Cao, J.; Yin, J.; Yuan, S.; Zhao, Y.; Li, J.; Zheng, N. Thiols as Interfacial Modifiers to Enhance the Performance and Stability of Perovskite Solar Cells. *Nanoscale* **2015**, *7* (21), 9443–9447.

(41) Hou, Y.; Aydin, E.; De Bastiani, M.; Xiao, C.; Isikgor, F. H.; Xue, D.-J.; Chen, B.; Chen, H.; Bahrami, B.; Chowdhury, A. H.; Johnston, A.; Baek, S.-W.; Huang, Z.; Wei, M.; Dong, Y.; Troughton, J.; Jalmood, R.; Mirabelli, A. J.; Allen, T. G.; Van Kerschaver, E.; Saidaminov, M. I.; Baran, D.; Qiao, Q.; Zhu, K.; De Wolf, S.; Sargent, E. H. Efficient Tandem Solar Cells with Solution-Processed Perovskite on Textured Crystalline Silicon. *Science* **2020**, *367* (6482), 1135–1140.

(42) Wu, Z.; Jiang, M.; Liu, Z.; Jamshaid, A.; Ono, L. K.; Qi, Y. Highly Efficient Perovskite Solar Cells Enabled by Multiple Ligand Passivation. *Adv. Energy Mater.* **2020**, *10* (10), 1903696.

(43) He, D.; Xu, X.; Liang, Z.; Niu, Y.; Sun, Y.; Gavin, T.; Falaras, P.; Hu, L. Defect Passivation and Humidity Protection for Perovskite Solar Cells Enabled by 1-Dodecanethiol. *J. Mater. Chem. C* **2021**, *9* (30), 9584–9591.

(44) Saliba, M.; Matsui, T.; Seo, J. Y.; Domanski, K.; Correa-Baena, J. P.; Nazeeruddin, M. K.; Zakeeruddin, S. M.; Tress, W.; Abate, A.; Hagfeldt, A.; Grätzel, M. Cesium-Containing Triple Cation Perovskite Solar Cells: Improved Stability, Reproducibility and High Efficiency. *Energy Environ. Sci.* **2016**, *9* (6), 1989–1997.

(45) Cao, D. H.; Stoumpos, C. C.; Malliakas, C. D.; Katz, M. J.; Farha, O. K.; Hupp, J. T.; Kanatzidis, M. G. Remnant PbI2, an Unforeseen Necessity in High-Efficiency Hybrid Perovskite-Based Solar Cells? *APL Mater.* **2014**, *2* (9), 091101.

(46) Chen, Q.; Zhou, H.; Song, T. Bin; Luo, S.; Hong, Z.; Duan, H. S.; Dou, L.; Liu, Y.; Yang, Y. Controllable Self-Induced Passivation of Hybrid Lead Iodide Perovskites toward High Performance Solar Cells. *Nano Lett.* **2014**, *14* (7), 4158–4163.

(47) Roose, B.; Dey, K.; Chiang, Y. H.; Friend, R. H.; Stranks, S. D. Critical Assessment of the Use of Excess Lead Iodide in Lead Halide Perovskite Solar Cells. *J. Phys. Chem. Lett.* **2020**, *11* (16), 6505–6512.

(48) Liu, Y.; Akin, S.; Hinderhofer, A.; Eickemeyer, F. T.; Zhu, H.; Seo, J.; Zhang, J.; Schreiber, F.; Zhang, H.; Zakeeruddin, S. M.; Hagfeldt, A.; Dar, M. I.; Grätzel, M. Stabilization of Highly Efficient and Stable Phase-Pure FAPbI3 Perovskite Solar Cells by Molecularly Tailored 2D-Overlayers. *Angew. Chemie* **2020**, *132* (36), 15818–15824.

(49) Tan, F.; Tan, H.; Saidaminov, M. I.; Wei, M.; Liu, M.; Mei, A.; Li, P.; Zhang, B.; Tan, C. S.; Gong, X.; Zhao, Y.; Kirmani, A. R.; Huang, Z.; Fan, J. Z.; Quintero-Bermudez, R.; Kim, J.; Zhao, Y.; Voznyy, O.; Gao, Y.; Zhang, F.; Richter, L. J.; Lu, Z. H.; Zhang, W.; Sargent, E. H. In Situ Back-Contact Passivation Improves Photovoltage and Fill Factor in Perovskite Solar Cells. *Adv. Mater.* **2019**, *31* (14), 1–6.

(50) Jin, J.; Li, H.; Chen, C.; Zhang, B.; Xu, L.; Dong, B.; Song, H.; Dai, Q. Enhanced Performance of Perovskite Solar Cells with Zinc Chloride Additives. *ACS Appl. Mater. Interfaces* **2017**, *9* (49), 42875–42882.

(51) Van Gompel, W. T. M.; Herckens, R.; Reekmans, G.; Ruttens, B.; D'Haen, J.; Adriaensens, P.; Lutsen, L.; Vanderzande, D. Degradation of the Formamidinium Cation and the Quantification of the Formamidinium-Methylammonium Ratio in Lead Iodide Hybrid Perovskites by Nuclear Magnetic Resonance Spectroscopy. *J. Phys. Chem. C* **2018**, *122* (8), 4117–4124.

SYNOPSIS TOC: